

Signal Temporal Logic Verification and Synthesis Using Deep Reachability Analysis and Layered Control Architecture

Joonwon Choi

CHOI774@PURDUE.EDU

School of Aeronautics and Astronautics, Purdue University, West Lafayette, IN 47907, USA

Kartik Anand Pant

KPANT@PURDUE.EDU

School of Aeronautics and Astronautics, Purdue University, West Lafayette, IN 47907, USA

Youngim Nam

NYI0944@UNIST.AC.KR

Department of Mechanical Engineering, Ulsan National Institute of Science and Technology, Ulsan, 44919, Republic of Korea

Henry Hellmann

HHELLMAN@PURDUE.EDU

School of Aeronautics and Astronautics, Purdue University, West Lafayette, IN 47907, USA

Karthik Nune

KNUNE@PURDUE.EDU

Interdisciplinary Engineering, Purdue University, West Lafayette, IN 47907, USA

Inseok Hwang

IHWANG@PURDUE.EDU

School of Aeronautics and Astronautics, Purdue University, West Lafayette, IN 47907, USA

Abstract

We propose a signal temporal logic (STL)-based framework that rigorously verifies the feasibility of a mission described in STL and synthesizes control to safely execute it. The proposed framework ensures safe and reliable operation through two phases. First, the proposed framework assesses the feasibility of STL by computing a backward reachable tube (BRT), which captures all states that can satisfy the given STL, regardless of the initial state. The proposed framework accommodates the multiple reach-avoid (MRA) problem to address more general STL specifications and leverages a deep neural network to alleviate the computation burden for reachability analysis, reducing the computation time by about 1000 times compared to a baseline method. We further propose a layered planning and control architecture that combines mixed-integer linear programming (MILP) for global planning with model predictive control (MPC) as a local controller for the verified STL. Consequently, the proposed framework can robustly handle unexpected behavior of obstacles that are not described in the environment information or STL, thereby providing reliable mission performance. Our numerical simulations demonstrate that the proposed framework can successfully compute BRT for a given STL and perform the mission.

Keywords: Signal temporal logic (STL), Reachability analysis, Model predictive control (MPC)

1. Introduction

Signal temporal logic (STL) is a specification language that can express a given specification of a target dynamical system using a combination of logic and temporal operators (Chen et al., 2018). STL can explicitly consider real-valued variables and dense-time requirements (Maler and Nickovic, 2004) and thus can precisely represent a specification in a formal manner. Thanks to this benefit, STL has been widely used by several machine learning algorithms to precisely represent spatio-temporal constraints or to enhance explainability (Leung et al., 2019; DeCastro et al., 2020; Leung et al., 2023; Puranic et al., 2021; Meng and Fan, 2023), alongside other temporal logic approaches. For instance, a linear temporal logic (LTL)-based method was proposed to monitor the safety of

LLM-based planner (Wang et al., 2024), whereas minimal relaxation for STL-based planning was proposed in (Buyukkocak and Aksaray, 2025).

While STL feasibility can be verified by MILP optimization (e.g., Gurobi returning an irreducible inconsistent subset (IIS), Ghosh et al. (2016)), it remains point-based and only considers a given (set of) initial state of the system. In contrast, reachability analysis considers all the reachable states of a target system, providing set-based analysis results (Jiang et al., 2024; Arfvidsson et al., 2024). Particularly, Chen et al. (2018) demonstrated that STL satisfaction can be examined using the backward reachable tube (BRT). However, general reachability analysis typically considers a single target-constraint set and thus, one might not be able to rigorously analyze STL involving multiple intermediate waypoints. Furthermore, computing BRT involves solving the Hamilton-Jacobi (HJ) PDE, suffering from the curse of dimensionality. To tackle this problem, deep learning-based methods have been actively investigated to alleviate the high computation burden (Bansal and Tomlin, 2021). Meanwhile, even if the STL itself is verified to be feasible, unexpected environmental changes or incorrect information may cause problems. For instance, there may be an unobserved obstacle, or the target state may differ from the known information. To address this issue, several algorithms have been proposed to fix STL specifications or to synthesize safe control inputs (Mallozzi et al., 2022; Buyukkocak and Aksaray, 2022).

Motivated by the aforementioned problems, we propose an end-to-end STL verification and control synthesis framework that efficiently confirms the feasibility and robustly executes a given STL mission. The proposed framework can be divided into two parts: *DeepSTLReach* for STL verification and *Layered-architecture* for planning and control. *DeepSTLReach* provides a *set of initial states* that can satisfy a given STL specification, considering the capability of a target dynamical system. Thus, one can obtain more comprehensive analysis results than by verifying a specific initial state or trajectory. Moreover, *DeepSTLReach* addresses the multiple reach-avoid (MRA) problem (Chen et al., 2025a,b) to resolve the conflict due to multiple unordered target-constraint sets of STL specifications. Interpreting STL from a reachability perspective may yield multiple target sets without a specific order for visiting (Chen et al., 2018), thereby often making it infeasible to formulate as a standard reachability analysis. On the other hand, MRA considers the reachability for visiting a sequence of multiple target-constraint sets. Accordingly, one can examine the feasibility of a broader range of STL specifications. Furthermore, to reduce computational time, we employ a deep learning-based approach to compute the BRT. Motivated by (Bansal and Tomlin, 2021), we train a neural network to obtain BRT through supervised learning. Consequently, the proposed framework can compute BRT significantly faster, making it suitable for online monitoring of a dynamical system.

Subsequently, once we verify that the given STL is feasible, we formulate a trajectory-planning and tracking problem using a layered control architecture (Matni et al., 2024) combining MILP and nonlinear model predictive control (MPC), respectively. STL specifications are transformed into integer constraints via robustness, which serves as a measure of how well the constraints are satisfied. Using the MILP-based planning as the reference trajectory, we employ an MPC-based tracking controller that tracks the reference trajectory while locally enforcing safety constraints (e.g., in a warehouse, the position of some of the obstacles may change during the operations, which MILP planning may not consider at the beginning of the task; these runtime safety violations are handled by the MPC).

In summary, our main contributions in this paper are: 1) We propose *DeepSTLReach* to verify the feasibility of STL using reachability analysis. *DeepSTLReach* can address multiple unordered

target-constraint sets that might be inherent within the given STL specification by leveraging MRA. Thus, one can verify a broader range of STL specifications while considering the physical capability of a dynamical system; 2) We leverage deep reachability analysis to reduce the computational complexity to compute BRT. As a result, *DeepSTLReach* significantly reduces the computation time compared to a baseline algorithm; 3) We propose a layered planning and control architecture combining MILP for global planning, enforcing spatio-temporal constraints via STL specifications, and nonlinear MPC-based local planning and control to perform a mission with certified runtime safety assurance; and 4) We rigorously test the performance of the proposed framework through a set of illustrative numerical simulations.

The rest of the paper is organized as follows. In Section 2, the preliminaries on STL and reachability analysis are presented. Section 3 provides a detailed description of our proposed framework. In Section 4, the results of the numerical simulations and experiments are presented. Lastly, the conclusion is given in Section 5.

2. Preliminaries

Throughout the paper, we assume the dynamics of a target dynamical system is given as:

$$\dot{x} = f(x, t, u, d) \quad (1)$$

where $x \in \mathbb{R}^n$ is the state, $u \in \mathbb{R}^m$ is the control input, $d \in \mathbb{R}^e$ is the disturbance, t is time, and $f(\cdot)$ is the dynamic model of the system.

2.1. Signal temporal logic (STL)

The syntax of STL can be represented using $T \mid P \mid \neg\phi \mid \phi_1 \wedge \phi_2 \mid \phi_1 \mathcal{U}_{[a,b]} \phi_2$, where $\phi(\cdot)$ is STL formula, T is logical true, P is a predicate, \neg is Boolean negation, \wedge is conjunction, and $\mathcal{U}_{[a,b]}$ is the *until* operator with $a \leq b \in \mathbb{R}$. The other operators also can be represented using the aforementioned syntax such as *disjunction* ($\vee, \neg(\neg\phi_1 \wedge \neg\phi_2)$), *eventually* ($\diamond, T\mathcal{U}_{[a,b]}\phi$), and *always* ($\square, \neg\diamond_{[a,b]}\neg\phi$) (Leahy et al., 2023). The satisfaction of such an STL can be represented using *robustness*, $\rho(x, t, \phi)$, a quantitative semantics of STL (Donzé and Maler, 2010), which is defined as:

$$\rho(x, t, \pi(x(t)) \geq c) := \pi(x(t)) - c \quad (2)$$

$$\rho(x, t, \neg\phi) := -\rho(x, t, \phi) \quad (3)$$

$$\rho(x, t, \phi_1 \wedge \phi_2) := \min(\rho(x, t, \phi_1), \rho(x, t, \phi_2)) \quad (4)$$

$$\rho(x, t, \phi_1 \mathcal{U}_{[a,b]} \phi_2) := \max_{t' \in [t+a, t+b]} \min(\rho(x, t', \phi_2), \min_{t'' \in [t, t']} \rho(x, t'', \phi_1)) \quad (5)$$

with respect to the state x at time t . If $\rho(x, t, \phi) > 0$, this means STL ϕ is satisfied at the state x and time t . Unless stated otherwise, we write $\rho(x, 0, \phi)$ as $\rho_\phi(x)$ for brevity throughout the paper.

2.2. Backward reachable tube (BRT)

To verify the feasibility of an STL, we use BRT, which captures all states that the target system can reach to a target within an arbitrary time horizon. The maximal BRT $\mathcal{R}^M(t, T; \mathcal{T}(\cdot), \mathcal{C}(\cdot))$, of (1) is defined as (Chen et al., 2018):

$$\begin{aligned} \mathcal{R}^M(t, T; \mathcal{T}(\cdot), \mathcal{C}(\cdot)) = \{x : \exists u(\cdot) \in \mathbb{U}, \forall d(\cdot) \in \mathbb{D}, \exists s \in [t, T], \\ \xi_{x,t}^{u(\cdot), d(\cdot)}(s) \in \mathcal{T}(s), \forall \tau \in [t, s], \xi_{x,t}^{u(\cdot), d(\cdot)}(\tau) \in \mathcal{C}(\tau)\} \quad (6) \end{aligned}$$

where $\xi_{x,t}^{u(\cdot),d(\cdot)}$ is the trajectory that starts from state x and time t following the control input $u(\cdot)$ with disturbance $d(\cdot)$. \mathbb{U} and \mathbb{D} denote the spaces of all admissible control inputs and disturbances, respectively; \mathcal{T} is the target set; and \mathcal{C} is the constraint set. \mathcal{R}^M is a sublevel set of the Bellman value function, i.e., $\mathcal{R}^M(t, T; \mathcal{T}(\cdot), \mathcal{C}(\cdot)) = \{x : h_{\mathcal{R}^M}(t, x) < 0\}$ where $h_{\mathcal{R}^M}(t, x)$ is defined as follows for given $h_{\mathcal{T}}(t, x)$ and $h_{\mathcal{C}}(x)$ of the target and constraint, respectively (Chen et al., 2018):

$$h_{\mathcal{R}^M}(t, x) = \inf_{u(\cdot) \in \mathbb{U}} \sup_{d(\cdot) \in \mathbb{D}} \min_{s \in [t, T]} \max\{h_{\mathcal{T}}(t, \xi_{x,t}^{u(\cdot),d(\cdot)}(s)), \max_{\tau \in [t, s]} h_{\mathcal{C}}(\xi_{x,t}^{u(\cdot),d(\cdot)}(\tau))\} \quad (7)$$

$h_{\mathcal{R}^M}(t, x)$ can be computed by solving the Hamilton–Jacobi Variational Inequality (HJ-VI). Similarly, the minimal BRT can be defined as

$$\mathcal{R}^m(t, T; \mathcal{T}(\cdot)) = \{x : \forall u(\cdot) \in \mathbb{U}, \exists d(\cdot) \in \mathbb{D}, \exists s \in [t, T], \xi_{x,t}^{u(\cdot),d(\cdot)}(s) \in \mathcal{T}(s)\}. \quad (8)$$

Similar to ρ_ϕ , we write $h_{(\cdot)}(0, x)$ as $h_{(\cdot)}(x)$ for brevity throughout the paper.

In Chen et al. (2018), BRT is investigated to compute the set of states that can satisfy given STL specification. Let \mathcal{S}_ϕ be a set of states that satisfy the STL ϕ . In other words, $(\xi_{x,t}^{u(\cdot),d(\cdot)}(\cdot), s) \models \phi \Leftrightarrow \xi_{x,t}^{u(\cdot),d(\cdot)}(s) \in \mathcal{S}_\phi$. From the definition of ρ , it is clear that $\mathcal{S}_\phi := \{x : \rho_\phi(x) > 0\}$. Then, the robustness (ρ) and Bellman value function of \mathcal{S}_ϕ ($h_{\mathcal{S}_\phi}$) have the following correspondence:

$$\rho_\phi(x) > 0 \Leftrightarrow h_{\mathcal{S}_\phi}(x) < 0 \quad (9)$$

In other words, a feasible set of states that satisfy the given STL ϕ (\mathcal{S}_ϕ) can be computed using a reachability formulation. Intuitively, one can compute the set of initial states in which a target system can accomplish a mission described by STL (ϕ) by computing (6).

Moreover, based on (2)-(5) and \wedge and \vee satisfy the followings relationship: $h_{\mathcal{S}_{\phi_1 \wedge \phi_2}}(x) = \max(h_{\mathcal{S}_{\phi_1}}(x), h_{\mathcal{S}_{\phi_2}}(x))$ and $h_{\mathcal{S}_{\phi_1 \vee \phi_2}}(x) = \min(h_{\mathcal{S}_{\phi_1}}(x), h_{\mathcal{S}_{\phi_2}}(x))$ (Chen et al., 2018). Such a correspondence between STL and BRT can further express various operators, including *until*, *eventually*, and *always*. For *until* operator, $\phi_1 \mathcal{U}_{[t_1, t_2]} \phi_2$, if we define a target set and constraint set as

$$\mathcal{T}_{\phi_2} = \begin{cases} \{x : (x(\cdot), s) \models \phi_2\}, & \text{if } t \in [s + t_1, s + t_2] \\ \emptyset & \text{otherwise,} \end{cases} \quad C_{\phi_1} = \{x : (x(\cdot), s) \models \phi_1\}, \quad (10)$$

the corresponding BRT can be defined as $\mathcal{R}^M(t, T, \mathcal{T}_{\phi_2}(\cdot), C_{\phi_1}(\cdot))$ from (7), i.e., one can compute $h_{\mathcal{R}^M} = h_{\mathcal{S}_{\phi_1 \mathcal{U}_{[t_1, t_2]} \phi_2}}$. *Eventually* can be computed by setting $\phi_1 = \emptyset$, i.e., $\diamond_{[t_1, t_2]} \phi = \emptyset \mathcal{U}_{[t_1, t_2]} \phi$.

Always requires the minimal BRT computation (8). For $\square_{[t_1, t_2]} \phi$, one can set

$$\mathcal{T}_\phi = \begin{cases} \{x : (x(\cdot), s) \not\models \phi\}, & \text{if } t \in [s + t_1, s + t_2] \\ \emptyset & \text{otherwise.} \end{cases} \quad (11)$$

along with the corresponding minimal BRT $\mathcal{R}^m(t, T; \mathcal{T}_\phi(\cdot))$. Then, $h_{\mathcal{S}_{\square_{[t_1, t_2]} \phi}}$ can be defined as $\{x : \notin \mathcal{R}^m(t, T; \mathcal{T}_\phi(\cdot))\}$, i.e., the complement of the minimal BRT.

3. Proposed framework

3.1. Framework overview

The objective of the proposed framework is to verify whether a given STL specification is feasible, safe, and executable by a target dynamical system, and to synthesize control while satisfying all requirements, even under unexpected changes. The proposed framework can largely be divided into two parts: 1) *DeepSTLReach*, a deep reachability-based STL verification algorithm, and 2) MILP-based planning and MPC-based control.

Unlike existing STL-based algorithms or planners, *DeepSTLReach* performs set-based analysis, i.e., it provides a set of states that can satisfy the given STL specification. Thus, one can easily determine whether an arbitrary initial state is feasible for the mission by checking whether it is included in the set, or use this information to select the optimal deployment option according to the preference.

Once the initial state and a feasible mission plan are chosen, we perform planning and control synthesis using a layered architecture that combines MILP-based global planning at a higher layer of abstraction with MPC-based local planning and control. The main advantage of our proposed architecture is that, even if environmental changes render the global plan infeasible, the local layer can accommodate runtime variabilities. We will highlight the details in the subsequent section.

3.2. Deep Reachability-based STL verification using DeepSTLReach

Extended from the existing algorithm (Chen et al., 2018), *DeepSTLReach* can deal with the conflict raised by *eventually* or *until* operator by leveraging MRA formulation. Furthermore, we utilize a neural network to reduce the computation burden for the reachability analysis, which can provide stable real-time verification performance.

3.2.1. ACCOMMODATING MRA PROBLEM

Although the feasibility of individual STL subformula can be tested using BRT, this result might introduce a conflict between subformulas. For instance, $\diamond_{[0,T]}A \wedge \diamond_{[0,T]}B$ requires to visit both A and B within time window $[0, T]$. However, *and* operation of the BRTs ($h_{S_{\diamond_{[0,T]}A \wedge \diamond_{[0,T]}B}} = \max(h_{S_{\diamond_{[0,T]}A}}, h_{S_{\diamond_{[0,T]}B}})$) might not guarantee the satisfaction of the STL specification, but merely an intersection of BRT for each individual subformula ($\diamond_{[0,T]}A, \diamond_{[0,T]}B$) (Chen et al., 2018). To address this issue, *DeepSTLReach* leverages MRA formulation. Motivated by (Chen et al., 2025b), *DeepSTLReach* begins by isolating STL subformulas that contain redundancy. More specifically, *DeepSTLReach* collects *eventually* (\diamond) and *until* (\mathcal{U}) operator along with the corresponding target and constraint set, using equations (10)-(11).

Assume there exists a total of N_{MRA} target-constraint sets, i.e., N_{MRA} *eventually* or *until* operators. *DeepSTLReach* then formulates all the possible ordering of N_{MRA} target-constraint sets and solve the respective MRA problem. For instance, for an arbitrary sequence of target-constraint sets with orders $\mathbb{T} = (\mathcal{T}_1, \dots, \mathcal{T}_{N_{MRA}})$ and $\mathcal{C} = (\mathcal{C}_1, \dots, \mathcal{C}_{N_{MRA}})$, let $h_{\mathcal{T}_i}$ and $h_{\mathcal{C}_i}$ be the functions correspond to \mathcal{T}_i and \mathcal{C}_i , respectively. Then, *DeepSTLReach* computes the BRT to visit the targets following the sequence \mathbb{T} as follows:

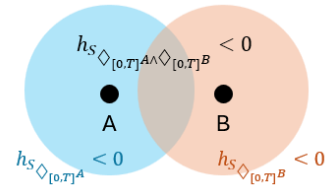


Figure 1: Example of conflict

1. Compute $h_{\mathcal{R}_{N_{MRA}}^M}(t, x)$ where $\mathcal{R}_{N_{MRA}}^M = \mathcal{R}_{N_{MRA}}^M(t, T; \mathcal{T}_{N_{MRA}}, \mathcal{C}_{N_{MRA}})$ based on (6) and (7). In other words, compute the BRT of the last target-constraint set.
2. For $i = 1, \dots, N_{MRA} - 1$, compute $\bar{h}_{\mathcal{T}_{N_{MRA}^M}^{MRA-i}}(t, x) = \max(h_{\mathcal{T}_{N_{MRA}^M}^{MRA-i}}, h_{\mathcal{R}_{N_{MRA}^M}^{MRA-i+1}})(t, x)$. Then, compute $h_{\mathcal{R}_{N_{MRA}^M}^{MRA-i}}(t, x)$ where $\mathcal{R}_{N_{MRA}^M}^{MRA-i} = \mathcal{R}_{N_{MRA}^M}^{MRA-i}(t, T; \bar{\mathcal{T}}_{N_{MRA}^M}^{MRA-i}, \mathcal{C}_{N_{MRA}^M}^{MRA-i})$ with $\bar{\mathcal{T}}_{N_{MRA}^M}^{MRA-i} = \{x : \bar{h}_{\mathcal{T}_{N_{MRA}^M}^{MRA-i}}(t, x) < 0\}$, i.e., iteratively computes the BRT backward over the given sequence (Chen et al., 2025b).

The last BRT computed from the above process (\mathcal{R}_1^M) represents the set of states that can satisfy the STL specifications with the sequential visit of (\mathbb{T}, \mathbb{C}) . Accordingly, one can compute the BRT for each respective sequence.

Let the computed BRT for $(\mathbb{T}_i, \mathbb{C}_i)$ from the above process as $\mathcal{R}_{\mathbb{T}_i, \mathbb{C}_i}^M$. Then, one can utilize the union of all the possible orderings of (\mathbb{T}, \mathbb{C}) , $\bigcup_{i=1}^M \mathcal{R}_{\mathbb{T}_i, \mathbb{C}_i}^M$, as a corresponding BRT for the collected subformulas with the *eventually* or *until* operator. The remaining subformulas without the *eventually* or *until* operator can be handled by (9)-(11), as shown in (Chen et al., 2018).

If a subformula has the nested form, i.e., it contains sets of *until* or *eventually* operators within other operators, one can iteratively apply the above process. Although this process might require numerous computations of BRT as N_{MRA} grows, *DeepSTLReach* can efficiently handle this problem using deep learning-based reachability analysis, which will be introduced in the following section.

3.2.2. DEEP REACHABILITY ANALYSIS

To address the computational complexity of solving HJ-VI, *DeepSTLReach* approximates the Bellman value function using a deep neural network in a supervised manner (Niarchos and Lygeros, 2006). More specifically, we first solve the HJ-VI using (Chen et al., 2018) and generate a training dataset $\mathcal{D} := \{(t_j, x_k, h_{\mathcal{R}^M}(t_j, x_k))\}$ where (t_j, x_k) spans all points of the discretized state-time grid. Let $\tilde{h}_\theta(t, x)$ denote a neural approximation of $h_{\mathcal{R}^M}(t, x)$, parameterized by a fully-connected multilayer perceptron (MLP) that takes (t, x) as input and outputs a scalar approximation. θ is trained to minimize a regression loss augmented with a conservative penalty:

$$\mathcal{L}(\theta) = \mathcal{L}_{\text{MSE}} + \mathcal{L}_{\text{penalty}}, \quad (12)$$

where

$$\begin{aligned} \mathcal{L}_{\text{MSE}} &= \mathbb{E}_{(t,x) \sim \mathcal{D}} \left[\left(\tilde{h}_\theta(t, x) - h_{\mathcal{R}^M}(t, x) \right)^2 \right], \\ \mathcal{L}_{\text{penalty}} &= \lambda \mathbb{E}_{(t,x) \sim \mathcal{D}} \left[\mathbf{1}_{\{h_{\mathcal{R}^M}(t,x) > 0\}} \max(0, \varepsilon - \tilde{h}_\theta(t, x)) \right], \end{aligned}$$

with \mathcal{L}_{MSE} denoting the supervised regression loss over \mathcal{D} , while $\mathcal{L}_{\text{penalty}}$ enforces conservative approximation in unsafe regions to prevent false-safe predictions. The penalty discourages underestimation of the value function when $h_{\mathcal{R}^M}(t, x) > 0$, thereby promoting a conservative approximation of the BRT boundary. Once trained, the maximal BRT can be evaluated in real time via the sublevel condition $\tilde{h}_\theta(t, x) < 0$, enabling online feasibility monitoring without solving the HJ-VI during runtime. The similar process can be applied for \mathcal{R}^m .

3.3. Layered-architecture for planning and control

Our proposed layered planning architecture can again be decomposed into two layers: *Global planning via MILP*, which ensures that STL specifications are met by the agent, and *MPC-based local planning and control*, which enables runtime safety assurance even when the initial plan becomes unsafe during the mission execution.

3.3.1. GLOBAL PLANNING VIA MIXED-INTEGER LINEAR PROGRAMMING (MILP)

Once the STL is verified to be feasible, we can transform the given STL specification to the constraints of a MILP problem (Belta and Sadraddini (2019); Raman et al. (2014)) via a robustness ρ . Given the dynamics of the target system (1), trajectory length N , and STL ϕ ; we denote $x(k|t)$ and $u(k|t)$ as the k^{th} step forward prediction of the state and inputs at time t , respectively. Here, $k \in \{1, \dots, N\}$ and we define $x(0|t) = x(t)$, $\mathbf{u}^{N,t} = [u(0,t)^\top, \dots, u(N|t)^\top]^\top$, and $\mathbf{x}(x(t), \mathbf{u}^{N,t}) = [x(0,t)^\top, \dots, x(N|t)^\top]^\top$. The optimization problem for motion planning with STL specification as constraints, i.e., for any arbitrary initial states $x(t)$ within the BRT, can be described as:

$$\min_{\mathbf{u}^{N,t}} J(\mathbf{x}(x(t), \mathbf{u}^{N,t}), \mathbf{u}^{N,t}) \quad (13)$$

$$\text{s.t. } \dot{x} = f(x, t, u) \quad (14)$$

$$\rho(x(t), t, \phi) \geq 0, \dots, \rho(x(t+N), t, \phi) \geq 0 \quad (15)$$

where $J(\cdot)$ is the cost function that incorporates mission planning and control objectives. Let the optimal state trajectories be denoted as $\bar{\mathbf{x}}$. These trajectories will be fed to the MPC-based tracking controller described later.

Equations (13)-(15) can be rewritten as a mixed integer formulation by appropriately encoding the predicates of the STL as mixed integer constraints (Raman et al. (2014)). For each predicate of the form $\pi = (a_\pi^\top x(t) \leq b_\pi)$, we define a variable $z(t)^\pi \in \{0, 1\}$ such that 1 (respectively, 0) stands for true (respectively, false). Dropping the time index and parameters for each of the variables for brevity, the relation between z^π , robustness ρ , and state x can be described as $a_\pi^\top x - M(1 - z^\pi + \rho) \leq b_\pi$ and $a_\pi^\top x + Mz^\pi + \rho \geq b_\pi$. The conversion of a compound STL formula to MILP constraints is performed recursively, which is omitted for brevity (see (Belta and Sadraddini (2019); Raman et al. (2014)) for more details).

3.3.2. MPC-BASED LOCAL PLANNING AND CONTROL

We adopt the MPC framework (Rawlings et al., 2017) augmented with control barrier functions (MPC-CBF) to perform local planning and control. The objective is to design a tracking controller that follows the reference trajectory $\bar{\mathbf{x}}$ generated by the MILP planner and also satisfies the STL specification. However, to ensure safety in the presence of runtime safety violations, we employ an MPC with state constraints that enforce system safety, since replanning with MILP can be computationally expensive. The continuous-time system dynamics are discretized using a fixed sampling period, and the resulting discrete-time model is employed within the MPC framework to compute control inputs at each sampling instant.

Let $\mathbf{x}_{l|k}$ and $\mathbf{u}_{l|k}$ denote the predicted state and control input at prediction step l computed at time k , with $l \in \{0, \dots, N\}$. The prediction horizon length is N , and $\mathbf{x}_{0|k} = \mathbf{x}_k$. The stacked

control sequence is defined as $\mathbf{u} = [u_{0|k}^\top \quad u_{1|k}^\top \quad \cdots \quad u_{N-1|k}^\top]^\top$. The MPC optimization problem is formulated as:

$$J^*(\mathbf{x}_k) = \min_{\mathbf{u}} \quad \|\mathbf{x}_{N|k} - \bar{\mathbf{x}}_{N|k}\|_P^2 + \sum_{l=0}^{N-1} \|\mathbf{x}_{l|k} - \bar{\mathbf{x}}_{l|k}\|_Q^2 + \|\mathbf{u}_{l|k} - \mathbf{u}_{l-1|k}\|_R^2 \quad (16a)$$

$$\text{s.t.} \quad \mathbf{x}_{0|k} = \mathbf{x}_k, \quad (16b)$$

$$\mathbf{x}_{l+1|k} = \bar{f}(\mathbf{x}_{l|k}, \mathbf{u}_{l|k}) \forall l = 0, \dots, N-1, \quad (16c)$$

$$(\mathbf{x}_{l|k}, \mathbf{u}_{l|k}) \in \mathcal{Z}, \quad (16d)$$

$$\mathbf{x}_{N|k} \in \Gamma, \quad (16e)$$

$$h^j(\mathbf{x}_{l|k}, \mathbf{u}_{l|k}) \geq 0, \quad \forall j = 1, \dots, m. \quad (16f)$$

where P , Q , and R are positive-definite weighting matrices of appropriate dimensions. $\bar{f}(\cdot)$ denotes the discrete-time system dynamics, \mathcal{Z} represents admissible state and input constraints, and Γ is a terminal invariant set. Finally, $h^j(\cdot)$ denotes the safety constraints (e.g., collision avoidance constraints). This formulation ensures recursive feasibility, reference-tracking performance, and provable safety by integrating state constraints.

Remark 1 *The result of DeepSTLReach can be easily integrated as a safety constraint $h^j(\cdot)$ in (16f) as the basis of the neural CBFs (So et al. (2024)) or control barrier value functions (Choi et al. (2021)). Such an extension will be investigated as future work.*

4. Numerical Simulation

4.1. Simulation setup

In this section, we validate the effectiveness of our proposed framework using illustrative numerical simulations. Throughout the simulations, we set the state and input of a target dynamical system as

$$x = [p_x, p_y, \dot{p}_x, \dot{p}_y]^T, \quad u = [\ddot{p}_x, \ddot{p}_y]^T \quad (17)$$

where p_x and p_y are the x and y-axis position, respectively. The dynamics of the system is defined as $\dot{x} = Ax + Bu$ with

$$A = \begin{bmatrix} \mathbf{I} & \mathbf{I} \\ \mathbf{0} & \mathbf{I} \end{bmatrix}, \quad B = \begin{bmatrix} \mathbf{0} \\ \mathbf{I} \end{bmatrix} \quad (18)$$

where \mathbf{I} and $\mathbf{0}$ are identity and zero matrix, respectively. We assume that environmental information (e.g., obstacle locations, waypoints, goal points) is known and available to all components of the framework, including BRT computation.

For *DeepSTLReach*, we train a network of four hidden layers with 128 neurons per layer and ReLU activation functions. The expectations in (12) are approximated using mini-batch stochastic gradient descent with the Adam optimizer. We set $\epsilon = 0.1$ and $\lambda = 0.05$ for the training.

All the computation times for the simulation scenarios are obtained using a computer equipped with an AMD Ryzen 7 8845HS processor and an NVIDIA RTX 4050 GPU. We implement each of our mission planning scenarios using the `stlpy` library (Kurtz and Lin (2022)) and the Gurobi solver (Gurobi Optimization, LLC (2024)), along with `stlcg` library (Leung et al. (2023)). The baseline BRT is computed by utilizing `hj-reachability` (git).

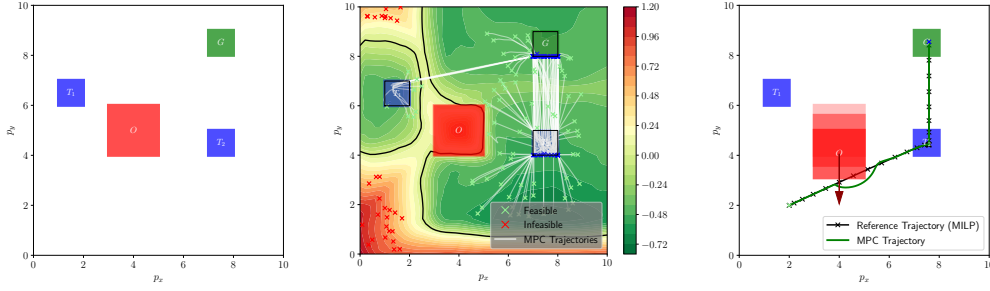


Figure 2: Simulation environment and results of Scenario 1. (Left) Scenario 1 map. (Center) Simulation result with $T = 8[s]$. (Right) Runtime assurance of MPC under unexpected environment changes with $T = 10[s]$

4.2. Scenario 1: Unexpected moving obstacle

In this section, we present the simulation results based on the scenario borrowed from (Kurtz and Lin, 2022) (Simulation Experiments (a)). For this scenario, we set $p_x, p_y \in [0, 15]$, $|\dot{p}_x| \leq 1$, $|\dot{p}_y| \leq 1$, $|\ddot{p}_x| \leq 0.5$, and $|\ddot{p}_y| \leq 0.5$. The STL specification is given as:

$$\diamond_{[0, T-5]}(\square_{[0, 5]}T_1 \vee \square_{[0, 5]}T_2) \wedge \square_{[0, T]} \neg O \wedge \diamond_{[0, T]}G, \quad (19)$$

where T is the mission time. The left figure of Fig. 2 shows the map of Scenario 1. There exist two waypoints (T_1 and T_2) represented as the blue boxes, one goal point (G , green), and one obstacle (O , red).

The center figure of Fig. 2 shows the simulation results. In the figure, the black line denotes the zero-level set boundary of the computed BRT; the green x denotes the feasible initial states; the white line denotes the trajectory generated by the MPC-based controller (16a); and the blue x denotes the final state of the trajectories. The red x denotes infeasible initial states, i.e., the MILP planner (13) cannot find a valid trajectory that satisfies the given STL (19). As shown the figure, the computed BRT from *DeepSTLReach* successfully identifies the infeasible region to perform the mission (19). Monte Carlo simulations with 100 randomly sampled initial states show that all states outside the BRT fail to find a feasible trajectory, whereas all states within the BRT succeed in finding a feasible trajectory using the proposed MPC controller.

Meanwhile, the right panel of Fig. 2 corresponds to the case in which the obstacle (O) moves downward, i.e., an unexpected environmental change occurs. As a result, the original plan generated by the MILP planner becomes infeasible, since its trajectory collides with the obstacle. Nevertheless, the proposed MPC controller accounts for environmental changes while satisfying the given STL specification, thereby enabling robust mission execution.

4.3. Scenario 2: Intersection

The STL specification given for Scenario 2 is defined as:

$$\square_{[0, T]}(\neg O_1 \wedge \neg O_2 \wedge \neg O_3) \wedge \square_{[0, T]}(r_1 \vee r_2) \wedge (\neg t_1 \mathcal{U}_{[0, T]}g_1) \wedge (\neg t_2 \mathcal{U}_{[0, T]}g_2), \quad (20)$$

with three obstacles ($O_1 - O_3$, red), two special regions (t_1 and t_2 , green boxes), and two goal points (g_1 and g_2) as shown in the left figure of Fig. 4. We set $p_x \in [-1, 1]$, $p_y \in [-2, 2]$, $|\dot{p}_x| \leq 0.3$, $|\dot{p}_y| \leq 0.3$, $|\ddot{p}_x| \leq 1$, and $|\ddot{p}_y| \leq 1$.

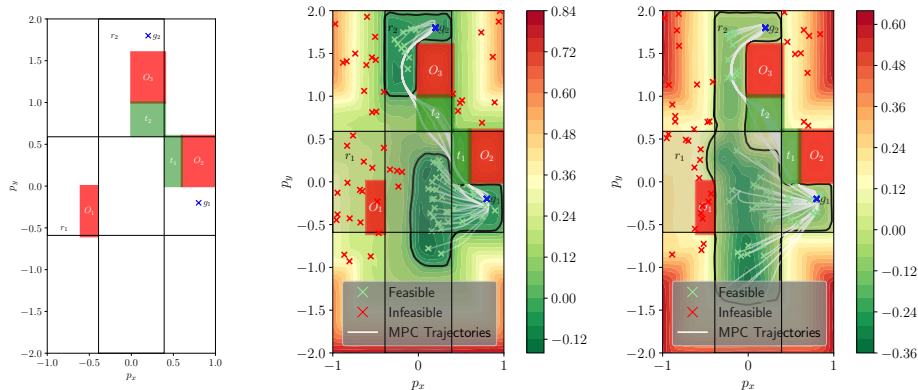


Figure 3: Simulation environment and results of Scenario 2. (Left) Scenario 2 map. (Center) Simulation result with $T = 10[s]$. (Right) Simulation result with $T = 11[s]$.

In this scenario, the dynamical system needs to visit g_1 and g_2 while staying within the union of r_1 ($|p_y| \leq 0.5$) and r_2 ($|p_x| \leq 0.5$) and avoiding three obstacles ($O_1 - O_3$). There are two special regions, t_1 and t_2 , into which the system cannot enter until it visits the corresponding goal point. The center and right figures of Fig. 3 show the simulation results. Similar to the previous simulation, the proposed framework successfully estimates the BRT with respect to the given STL, generating a valid trajectory using the proposed MPC controller to accomplish the mission.

4.4. Computation time comparison

Table 1 shows the computation time of *DeepSTLReach* for Scenarios 1 and 2 with $T = 10[s]$ and $T = 15[s]$, respectively. For the first row (Baseline), we use *hj_reachability* to compute BRT, whereas the second row (Proposed) uses the trained neural network with loss function (12). All the times are computed as the average of three independent computations. As shown in the table, the trained neural network achieves significantly faster performance, demonstrating the efficiency of the proposed framework.

Table 1: Computation time ([s])

	Scenario 1	Scenario 2
Baseline	39.488	9.153
Proposed	0.038	0.009

5. Conclusion

In this paper, we propose an STL-based framework for verifying feasibility and executing STL missions. *DeepSTLReach* verifies the specification by computing the BRT via deep reachability analysis, providing comprehensive feasibility information, including *where to start the mission*, rather than verifying only a specific initial state. Furthermore, our layered architecture combines global and local planning to ensure system safety even if the initial plan’s feasibility changes during execution. Numerical simulations validate the proposed framework’s ability to efficiently verify STL specifications. Future work will address the scalability of *DeepSTLReach* by employing neural PDE techniques and integrating the BRT with a sampling-based global planner to enable faster global replanning in response to large environmental changes.

Acknowledgments

This material is based on work supported by the National Science Foundation under Grant Number CNS-1836952. Any opinions, findings, conclusions, or recommendations expressed in this work are those of the authors and do not necessarily reflect the views of the National Science Foundation.

References

https://github.com/StanfordASL/hj_reachability.

Kaj Munhoz Arfvidsson, Frank J Jiang, Karl H Johansson, and Jonas Mårtensson. Ensuring safety at intelligent intersections: Temporal logic meets reachability analysis. In *2024 IEEE Intelligent Vehicles Symposium (IV)*, pages 292–298. IEEE, 2024.

Somil Bansal and Claire J Tomlin. Deepreach: A deep learning approach to high-dimensional reachability. In *2021 IEEE International Conference on Robotics and Automation (ICRA)*, pages 1817–1824. IEEE, 2021.

Calin Belta and Sadra Sadraddini. Formal methods for control synthesis: An optimization perspective. *Annual Review of Control, Robotics, and Autonomous Systems*, 2(1):115–140, 2019.

Ali Tevfik Buyukkocak and Derya Aksaray. Temporal relaxation of signal temporal logic specifications for resilient control synthesis. In *2022 IEEE 61st Conference on Decision and Control (CDC)*, pages 2890–2896. IEEE, 2022.

Ali Tevfik Buyukkocak and Derya Aksaray. Resilient online planning for mobile robots with minimal relaxation of signal temporal logic specifications. *IEEE Robotics and Automation Letters*, 2025.

Mo Chen, Qizhan Tam, Scott C Livingston, and Marco Pavone. Signal temporal logic meets reachability: Connections and applications. In *International Workshop on the Algorithmic Foundations of Robotics*, pages 581–601, 2018.

Yu Chen, Shaoyuan Li, and Xiang Yin. Control synthesis for multiple reach-avoid tasks via hamilton-jacobi reachability analysis. In *2025 IEEE 64th Conference on Decision and Control (CDC)*, pages 5980–5985. IEEE, 2025a.

Yu Chen, Shaoyuan Li, and Xiang Yin. Control synthesis for multiple reach-avoid tasks via hamilton-jacobi reachability analysis. *arXiv preprint arXiv:2509.10896*, 2025b.

Jason J Choi, Donggun Lee, Koushil Sreenath, Claire J Tomlin, and Sylvia L Herbert. Robust control barrier–value functions for safety-critical control. In *2021 60th IEEE Conference on Decision and Control (CDC)*, pages 6814–6821. IEEE, 2021.

Jonathan DeCastro, Karen Leung, Nikos Aréchiga, and Marco Pavone. Interpretable policies from formally-specified temporal properties. In *2020 IEEE 23rd International Conference on Intelligent Transportation Systems (ITSC)*, pages 1–7. IEEE, 2020.

Alexandre Donzé and Oded Maler. Robust satisfaction of temporal logic over real-valued signals. In *International Conference on Formal Modeling and Analysis of Timed Systems*, pages 92–106. Springer, 2010.

Shromona Ghosh, Dorsa Sadigh, Pierluigi Nuzzo, Vasumathi Raman, Alexandre Donzé, Alberto L Sangiovanni-Vincentelli, S Shankar Sastry, and Sanjit A Seshia. Diagnosis and repair for synthesis from signal temporal logic specifications. In *Proceedings of the 19th International Conference on Hybrid Systems: Computation and Control*, pages 31–40, 2016.

- Gurobi Optimization, LLC. Gurobi Optimizer Reference Manual. <https://www.gurobi.com>, 2024.
- Frank J Jiang, Kaj Munhoz Arfvidsson, Chong He, Mo Chen, and Karl H Johansson. Guaranteed completion of complex tasks via temporal logic trees and hamilton-jacobi reachability. In *2024 IEEE 63rd Conference on Decision and Control (CDC)*, pages 5203–5210. IEEE, 2024.
- Vince Kurtz and Hai Lin. Mixed-integer programming for signal temporal logic with fewer binary variables. *arXiv preprint arXiv:2204.06367*, 2022.
- Kevin Leahy, Makai Mann, and Cristian-Ioan Vasile. Rewrite-based decomposition of signal temporal logic specifications. In *NASA Formal Methods Symposium*, pages 224–240. Springer, 2023.
- Karen Leung, Nikos Aréchiga, and Marco Pavone. Backpropagation for parametric STL. In *2019 IEEE Intelligent Vehicles Symposium (IV)*, pages 185–192. IEEE, 2019.
- Karen Leung, Nikos Aréchiga, and Marco Pavone. Backpropagation through signal temporal logic specifications: Infusing logical structure into gradient-based methods. *The International Journal of Robotics Research*, 42(6):356–370, 2023.
- Oded Maler and Dejan Nickovic. Monitoring temporal properties of continuous signals. In *International Symposium on Formal Techniques in Real-Time and Fault-Tolerant Systems*, pages 152–166. Springer, 2004.
- Piergiuseppe Mallozzi, Inigo Incer, Pierluigi Nuzzo, and Alberto Sangiovanni-Vincentelli. Contract-based specification refinement and repair for mission planning. *arXiv preprint arXiv:2211.11908*, 2022.
- Nikolai Matni, Aaron D Ames, and John C Doyle. Towards a theory of control architecture: A quantitative framework for layered multi-rate control. *arXiv preprint arXiv:2401.15185*, 2024.
- Yue Meng and Chuchu Fan. Signal temporal logic neural predictive control. *IEEE Robotics and Automation Letters*, 8(11):7719–7726, 2023.
- K. N. Niarchos and J. Lygeros. A neural approximation to continuous time reachability computations. In *Proceedings of the 45th IEEE Conference on Decision and Control*, pages 6313–6318, 2006. doi: 10.1109/CDC.2006.377358.
- Aniruddh Puranic, Jyotirmoy Deshmukh, and Stefanos Nikolaidis. Learning from demonstrations using signal temporal logic. In *Conference on Robot Learning*, pages 2228–2242. PMLR, 2021.
- Vasumathi Raman, Alexandre Donzé, Mehdi Maasoumy, Richard M. Murray, Alberto Sangiovanni-Vincentelli, and Sanjit A. Seshia. Model predictive control with signal temporal logic specifications. In *53rd IEEE Conference on Decision and Control*, pages 81–87, 2014. doi: 10.1109/CDC.2014.7039363.
- James Blake Rawlings, David Q Mayne, Moritz Diehl, et al. *Model predictive control: theory, computation, and design*, volume 2. Nob Hill Publishing Madison, WI, 2017.

Oswin So, Zachary Serlin, Makai Mann, Jake Gonzales, Kwesi Rutledge, Nicholas Roy, and Chuchu Fan. How to train your neural control barrier function: Learning safety filters for complex input-constrained systems. In *2024 IEEE International Conference on Robotics and Automation (ICRA)*, pages 11532–11539. IEEE, 2024.

Ziming Wang, Qingchen Liu, Jiahu Qin, and Man Li. Ensuring safety in llm-driven robotics: A cross-layer sequence supervision mechanism. In *2024 IEEE/RSJ International Conference on Intelligent Robots and Systems (IROS)*, pages 9620–9627. IEEE, 2024.

Appendix

6. Scenario 3: Door and key

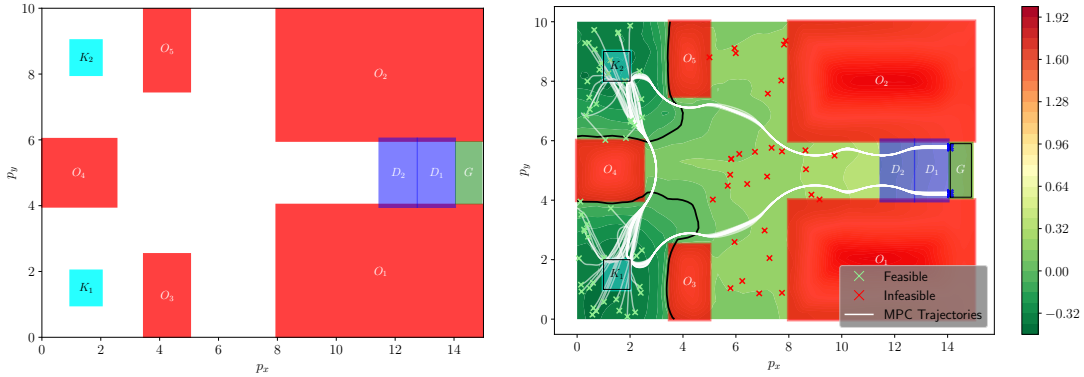


Figure 4: Simulation environment and results of Scenario 3. (Left) Scenario 3 map. (Right) Simulation result with $T = 20s$.

Similar to the previous simulation, Scenario 3 is set based on Kurtz and Lin (2022) (Simulation Experiment (d)). The STL specification given for Scenario 3 is defined as

$$\bigwedge_{i=1}^2 (\neg D_i \mathcal{U}_{[0,T]} K_i) \wedge \diamond_{[0,T]} G \wedge \square_{[0,T]} \left(\bigwedge_{i=1}^5 \neg O_i \right) \quad (21)$$

where K_i represents the key for door D_i , i.e., D_i opens only when the target system visits the corresponding K_i . The detailed map of Scenario 3 can be found in Fig. 4. For this scenario, we set $p_x \in [0, 15]$, $p_y \in [0, 10]$ $|\dot{p}_x| \leq 2$, $|\dot{p}_y| \leq 2$, $|\ddot{p}_x| \leq 0.5$, and $|\ddot{p}_y| \leq 0.5$. All other parameters are identical to those of the previous experiment.

7. Comparison of BRT between baseline and proposed framework

Figure 5 shows the comparison of computed BRT using the baseline and proposed framework. In the figure, the blue line represents the result from the baseline method and the red dashed line is the result from the proposed algorithm. All other conditions are identical to Section 4.

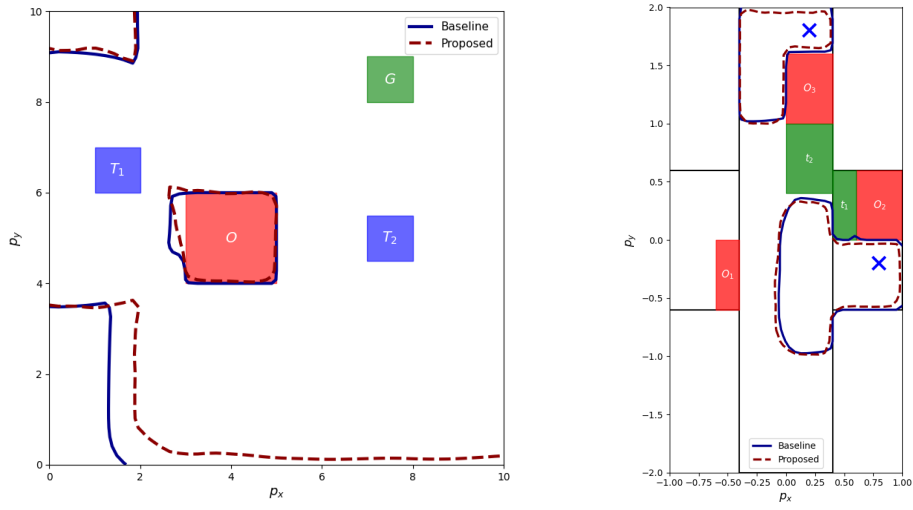


Figure 5: (Left) Scenario 1, $T = 9[s]$ (Right) Scenario 2, $T = 10[s]$